DOI: 10.1002/ejic.200701125

Mesolamellar Phases Containing $[Re_6Q_8(CN)_6]^{4-}$ (Q = Te, Se, S) Cluster Anions

Min-Jung Suh,[a] Vo Vien,[a] Seong Huh,[a] Youngmee Kim,[a] and Sung-Jin Kim*[a]

Keywords: Mesolamellar phases / Mesoscale materials / Surfactant-template assembly / Octahedral rhenium clusters

We synthesized new mesostructured materials through the surfactant-templated assembly of octahedral rhenium cluster $[Re_6Q_8(CN)_6]^{4-}$ (Q = Te, Se and S) anions. The mesostructured lamellar phases with the general formula $[C_nH_{2n+1}N(CH_3)_3]_4[Re_6Q_8(CN)_6]$ (n = 14, 16, 18; Q = Te, Se, S; **1**: n = 14, Q = Te; **2**: n = 16, Q = Te; **3**: n = 18, Q = Te; **4**: n = 16, Q = Se; **5**: n = 16, Q = S) were prepared by an ion exchange/precipitation reaction of alkyltrimethylammonium surfactants and the corresponding cluster $K_4[Re_6Q_8(CN)_6]$ in an H_2O/acetone medium at room temperature. The orange plate-like crystals of **1** and **4** were obtained by slow concentration of their solutions and their crystal structures determined by single-crystal X-ray diffraction. In the structure, the rhenium clusters form layers with a pseudo-hexagonal arrangement, and these inorganic layers are separated by a bilayer of interdigitated surfactant cations. Compounds **1**–**5** were characterized using powder X-ray diffraction, TEM, IR, Raman, FL, UV/Vis spectroscopy, and thermogravimetric analysis.

Introduction

The design and synthesis of new solid materials with controlled structures are of great interest in materials science. Since the discovery of a new family of mesoporous siliceous molecular sieves by Kresge et al. at Mobil Company in 1992,[1] the use of surfactants as soft structure-directing agents in the synthesis of hard inorganic materials has provided a versatile route to preparing numerous multifunctional mesoporous materials. Among ordered siliceous mesoscale materials, it has been well known that lamellar (MCM-50), hexagonal (MCM-41) and cubic (MCM-48) phases can all be prepared using appropriate surfactants and reaction conditions, and that they can be transformed into each other.[2] Recently, however, these lamellar, hexagonal and cubic phases were also prepared from non-oxidic germanium chalcogenide clusters.[3,4] However, the chemistry used to construct such non-oxidic frameworks is slightly different from that used in the silicate system. The lamellar phases were obtained predominantly by an ion exchange reaction between the germanium chalcogenide cluster molecules and the surfactants, while the hexagonal and cubic phases were constructed from the tetrahedral $[Ge_4S_{10}]^{4-}$ building units that are linked together through the transition metal cations in the presence of suitable surfactants. These mesostructures based on non-oxidic molecular clusters show promise in developing advanced applications in optoelectronic, photonic or magnetic fields that have been not found in the silica framework.

Very few lamellar phases consisting of metal clusters have been characterized by single-crystal X-ray diffraction: $[C_nH_{2n+1}N(CH_3)_3]_4Ge_4Q_{10}$ (Q = S, Se; n = 8–18),[4a,4b] $[C_nH_{2n+1}NH_3]_4Ge_4S_{10}$ (n = 12–18),[4c] $[C_{12}H_{25}NH_3]_4Sn_2S_6\cdot 2H_2O$,[5] $[C_{12}H_{25}N(CH_3)_3]_4H_2V_{10}O_{28}\cdot 8H_2O$,[6] $[C_{12}H_{25}N(CH_3)_3]_4V_{12}O_{32}\cdot 6H_2O$,[7] and $[C_{16}H_{33}N(CH_3)_3]_4SiMo_{12}O_{40}$.[8] Others that have been described from powder X-ray diffraction and TEM data include $[C_{16}H_{33}N(CH_3)_3]_6(H_2W_{12}O_{40})$, $[C_{16}H_{33}N(CH_3)_3]_{2+x}(Nb_xW_{6-x}O_{19})$[9] ($x$ = 2, 3, 4), $[C_{12}H_{25}N(CH_3)_3]_6NaPW_{11}O_{39}$,[10] and $(NH_4)_x(C_nH_{2n+1}NH_3)_y(NH_4V_2P_2BO_{12})_6\cdot 3H_2O$ ($7 \le n \le 18$; $x + y = 17$).[11]

The chemistry of hexarhenium chalcogenide clusters, $[Re_6Q_8(CN)_6]^{4-}$, has developed rapidly and produced an interesting number of structurally well-defined solid architectures in recent years.[12] These octahedral clusters possess interesting electronic and luminescence properties, and can be used as an analogue of tetrahedral building blocks such as $[Ge_4S_{10}]^{4-}$ and $[SnSe_4]^{4-}$ in design of new types of mesoporous materials[12b] possessing various useful physical properties. Moreover, the octahedral clusters have been combined with various metal cations or metal complexes to yield well-defined mesostructures, some of which have resulted in gas-storage materials, chemical sensors or catalysts.[13,14] However, no works have been reported relating octahedral metal chalcogenide clusters to the synthesis of ordered mesostructures templated with surfactants. Therefore, here we present a rational synthesis, including the properties of a new series of mesostructured materials pre-

[a] Division of Nano Sciences and Department of Chemistry, Ewha Womans University, Seoul 120-750, Korea
Fax: +82-2-3277-2384
E-mail: sjkim@ewha.ac.kr

pared by self-assembly of cluster $[Re_6Q_8(CN)_6]^{4-}$ (Q = Te, Se, S) in the presence of $C_nH_{2n+1}N(CH_3)_3Br$ (n = 14, 16, 18) acting as structure-directing agents: $[C_{14}H_{29}N(CH_3)_3]_4[Re_6Te_8(CN)_6]$ (**1**), $[C_{16}H_{33}N(CH_3)_3]_4[Re_6Te_8(CN)_6]$ (**2**), $[C_{18}H_{37}N(CH_3)_3]_4[Re_6Te_8(CN)_6]$ (**3**), $[C_{16}H_{33}N(CH_3)_3]_4[Re_6Se_8(CN)_6]$ (**4**) and $[C_{16}H_{33}N(CH_3)_3]_4[Re_6S_8(CN)_6]$ (**5**).

Results and Discussion

The reactions of $C_nH_{2n+1}N(CH_3)_3Br$ (n = 14, 16, 18) and $K_4[Re_6Q_8(CN)_6]$ (Q = Te, Se, S) led to several new surfactant-containing mesoscale rhenium cluster compounds. Upon mixing the alkyltrimethylammonium salt and the rhenium cluster solutions at an ambient temperature, the products precipitated immediately through the following ion-exchange reaction.

$$4\,[C_nH_{2n+1}N(CH_3)_3]Br + K_4[Re_6Q_8(CN)_6] \rightarrow [C_nH_{2n+1}N(CH_3)_3]_4[Re_6Q_8(CN)_6] + 4\,KBr$$

The crystal structures of **1** and **4** were determined in space group $P\bar{1}$, and a summary of the crystallographic data is given in Table 1. The structure of **1** is composed of alternating layers of $[Re_6Te_8(CN)_6]^{4-}$ clusters and tetradecyltrimethylammonium cations (Figure 1). The spacing value d for the structure of **1** is 22.20 Å, close to the 21.71 Å obtained from the PXRD data. Within the ab plane, the $[Re_6Te_8(CN)_6]^{4-}$ clusters form an array of nearly hexagonal arrangements, with each cluster surrounded by six neighbors; this is shown in Figure 2. The average distance between the centers of two neighboring Re_6 clusters is about 11.63 Å, with close contacts between the two neighboring N_{cyano} atoms ranging from 6.35 to 7.32 Å. The positively charged trimethylammonium head groups of the two crystallographically different molecules are positioned toward the negatively charged clusters. The layers of $[Re_6Te_8(CN)_6]^{4-}$ are separated by layers of surfactant chains arranged in an antiparallel way. The angle between the surfactant and rhenium cluster plane is about 39.80°, close to the 32.24° calculated for the relationship between the interlayer spacing d and the number of carbon atoms n in the surfac-

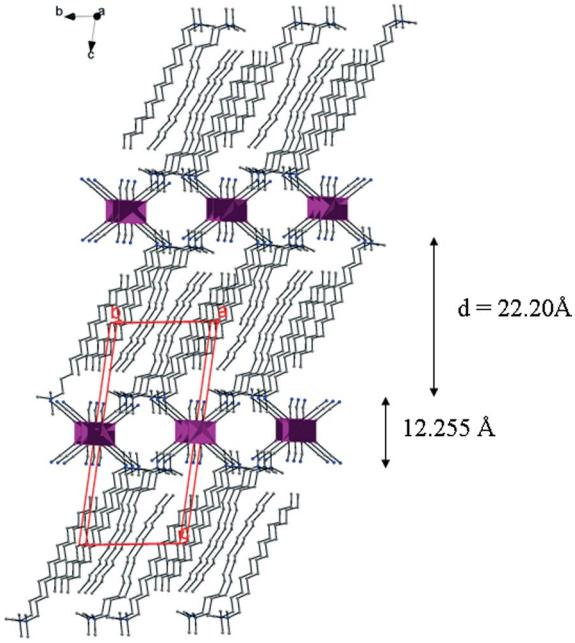

Figure 1. Overall structure of **1** viewed approximately along the a-axis. Re_6 cores are illustrated as dark red polyhedrons, with eight tellurium atoms capping the Re_6 core. H atoms are omitted for clarity.

Table 1. Crystal data and structure refinement for compounds **1** and **4**.

	1	**4**
Empirical formula	$[C_{14}H_{29}N(CH_3)_3]_4[Re_6Te_8(CN)_6]$	$[C_{16}H_{33}N(CH_3)_3]_4[Re_6Se_8(CN)_6]$
Formula mass	3320.06	3043.14
Temperature	293(2) K	293(2) K
Wavelength	0.71073 Å	0.71073 Å
Space group	triclinic, $P\bar{1}$	triclinic, $P\bar{1}$
Unit cell dimensions	a = 11.482(5) Å	a = 11.717(2) Å
	b = 11.625(5) Å	b = 11.844(2) Å
	c = 22.200(10) Å	c = 21.393(4) Å
	α = 78.244(8)°	α = 87.99(3)°
	β = 82.314(8)°	β = 87.59(3)°
	γ = 61.283(8)°	γ = 60.97(3)°
Volume	2542.1(19) Å^3	2593.2(9) Å^3
Z	1	1
Density (calculated)	2.169 Mg/m^3	1.949 Mg/m^3
Absorption coefficient	9.403 mm^{-1}	9.823 mm^{-1}
F(000)	1532	1452
Crystal size	0.10 × 0.10 × 0.10 mm	0.10 × 0.10 × 0.10 mm
Data/restraints/parameters	9767/0/450	9966/1/486
Goodness-of-fit on F^2	0.894	0.948
Final R indices [$I > 2\sigma(I)$]	R_1 = 0.0652	R_1 = 0.0708
	wR_2 = 0.1286	wR_2 = 0.1679
R indices (all data)	R_1 = 0.1727	R_1 = 0.1311
	wR_2 = 0.1611	wR_2 = 0.1989
Largest diff. peak and hole	1.986 and –1.345 e·Å^{-3}	2.417 and –2.557 e Å^{-3}

tant. Thus, we are able to prepare new lamellar materials consisting of inorganic layers separated by precisely tunable mesoscale distances by choosing surfactants of suitable chain lengths.

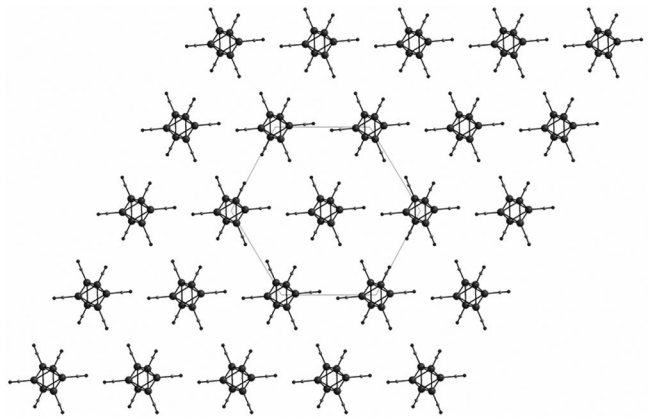

Figure 2. Pseudo-hexagonal two-dimensional packing of the $[Re_6Te_8(CN)_6]^{4-}$ clusters in **1**. The hexagon is in the figure. H and Te atoms are omitted for clarity.

The structure of **4** is essentially similar to that of **1**, as shown in Figure 3. The spacing value *d* for the structure of **4** is 21.51Å, which is shorter than that of **1**. Moreover, the tilt angle of the surfactants is 54.7°, which is larger than that of **1**. Compound **4** possesses a lamellar structure, as well as $[Re_6Se_8(CN)_6]^{4-}$ clusters with a very similar pseudo-hexagonal arrangement. Along the *c* direction, layers of Re_6 clusters alternate with bilayers of interdigitated surfactant cations. Figure 3 shows the layers of the interdigitated

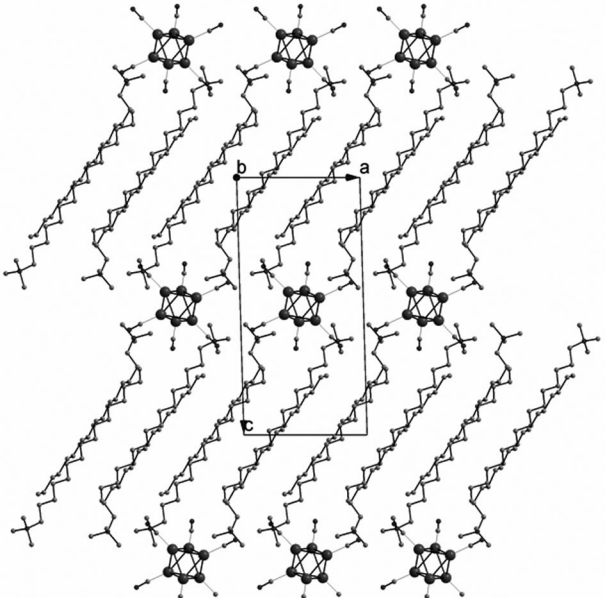

Figure 3. Overall structure of **4** viewed along the *b*-axis. H atoms are omitted for clarity. The structure of **4** is similar to that of **1**. However, the angle of the surfactants to the rhenium cluster plane in **4** is larger than that in **1**.

chains. The approximate distance between chains in the interdigitated region is 2.74–3.05 Å, as measured by the closest H···H distance between two neighboring chains.

The powder X-ray diffraction (PXRD) patterns of the surfactant–rhenium telluride $[Re_6Te_8(CN)_6]^{4-}$ cluster hybrid phases **1**, **2** and **3** clearly reveal strong (00l) reflections due to the lamellar character; this is shown in Figure 4. From these strong (00l) peaks the interlayer spacings of the three phases were calculated. A linear relationship between the interlayer spacing (*d*) and the number of carbon atoms (*n*) of the long alkyl groups (C_nH_{2n+1} in $[C_nH_{2n+1}N(CH_3)_3]^+$) is observed and expressed as $d = 0.6775n + 12.255$ (Å) (see Figure 5). This means that the average increment of interlayer spacing ($\Delta d/\Delta n$) is 0.6775 Å, smaller than the 1.27 Å length increment per carbon atom in a stretched form of the alkyl chain.[15] Therefore, hydrophobic alkyl chains of the surfactants in these materials may be arranged with a

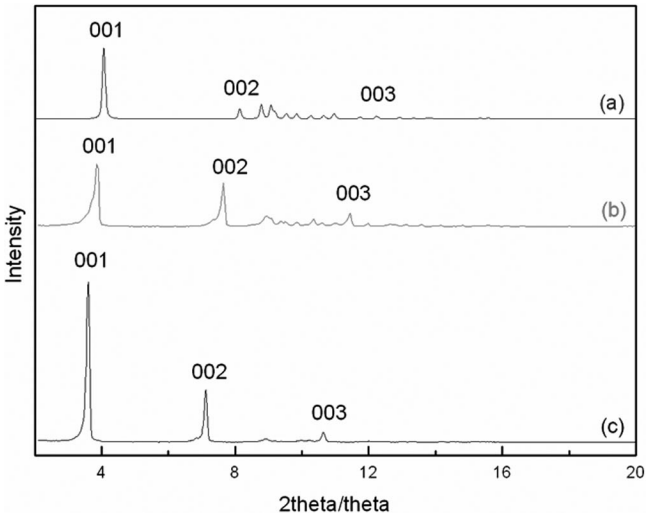

Figure 4. Powder X-ray diffraction patterns of lamellar (a) compound **1**, (b) compound **2**, and (c) compound **3**.

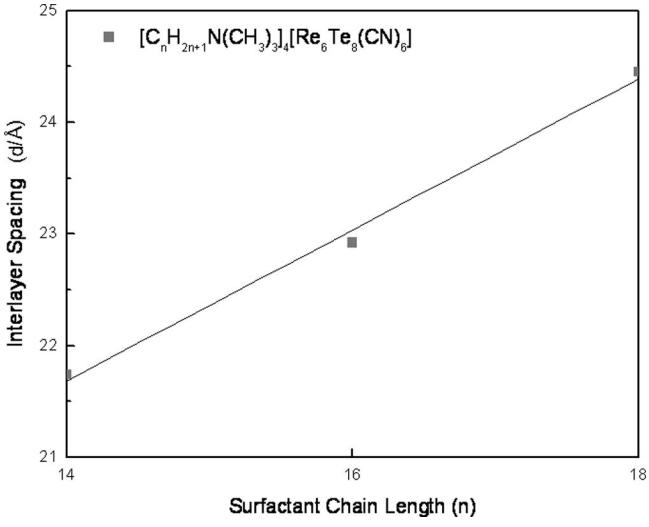

Figure 5. Variation of the interlayer spacing of $[C_nH_{2n+1}N(CH_3)_3]_4$-$[Re_6Q_8(CN)_6]$ with *n*.

large tilt angle of $\sin^{-1}(0.6775/1.27) \approx 32.24°$ (Figure 1). Extrapolation of the data to $n = 0$ gives an intercept of 12.255 (Å), which is smaller than the sum of the rhenium cluster and head group $(CH_3)_3NH^+$ of the surfactant. This may be explained by the strong direct anion–cation interaction between the cationic head groups of the surfactant and the anionic rhenium cluster.

The powder X-ray diffraction patterns of compounds **2**, **4** and **5** are compared in Figure 6. The lamellar-phase materials were synthesized using the same surfactant, cetyltrimethylammonium bromide, together with different rhenium chalcogenides, $[C_{16}H_{33}N(CH_3)_3]_4[Re_6Q_8(CN)_6]$ [Q = Te (**2**), Se (**4**) and S (**5**)]. The respective interlayer spacing values *d* of **2**, **4** and **5** are 22.92 Å, 21.32 Å, and 27.24 Å, respectively. The varying *d* values of the three chalcogenides analogues (S, Se, Te) indicate different tilt angles of the alkyl chains in $[C_{16}H_{33}N(CH_3)_3]_4[Re_6Q_8(CN)_6]$ (Q = S, Se, Te): The more covalent ligands, Se and Te, have larger tilt angles compared to the ionic sulfur ligand.

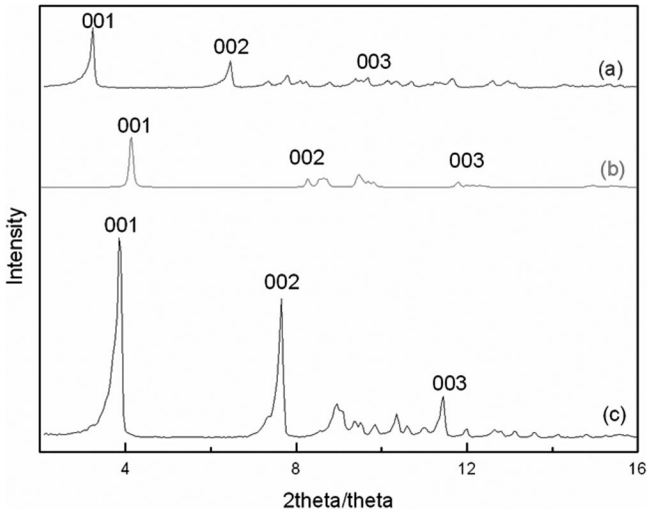

Figure 6. Comparison of powder X-ray diffraction patterns of lamellar (a) compound **5**, (b) compound **4**, and (c) compound **2**.

Figure 7 shows the TEM images of **2**, with highly aligned mesostructures clearly visible. The interlayer spacing value *d* of the image is about 22.2 Å, which sufficiently matches the *d* value (22.9 Å) obtained from the PXRD data. The electron diffraction pattern also proves that **2** is a lamellar phase.

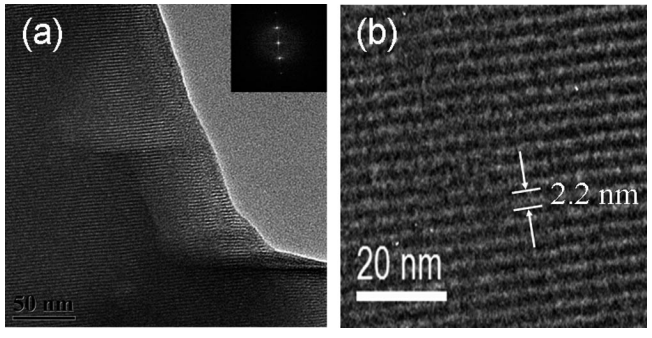

Figure 7. TEM images of **2**. (a) Electron diffraction pattern. (b) The interlayer spacing value *d* is about 22.2 Å.

To investigate the bonding features of these phases, **2** as a representative phase was characterized by IR spectroscopy, and the results are shown in Figure 8. For comparison, the IR spectra of the starting cluster $K_4[Re_6Te_8(CN)_6]$ and $C_{16}H_{33}N(CH_3)_3Br$ (CTABr) surfactant are also shown. Figure 8(a) reveals a characteristic strong band at 2090 cm^{-1} corresponding to the vibration mode of the cyanide group of the cluster, thus indicating that the cyanide groups exist in **2**.[14a] It also reveals the presence of CTA cations in **2** through comparison of the respective spectra of CTABr and the product. In addition, the position of the stretching bands of the CH_2 groups is worth noting from the spectra. It is well known that the positions of the asymmetric stretching band (2920 cm^{-1}) and the symmetric band (2850 cm^{-1}) of the CH_2 groups in *n*-alkyl chains are quite sensitive to chain conformation and that these two bands shift to lower wavenumbers if disorder (kink and gauche blocks) is introduced into the *n*-alkyl chains.[16] In the case of **2**, the spectrum exhibits two separate bands at 2920 and 2850 cm^{-1}, which are very close to those of the CTABr. This means that the *n*-alkyl chains remain in ordered conformation in the interlayer space of **2**.

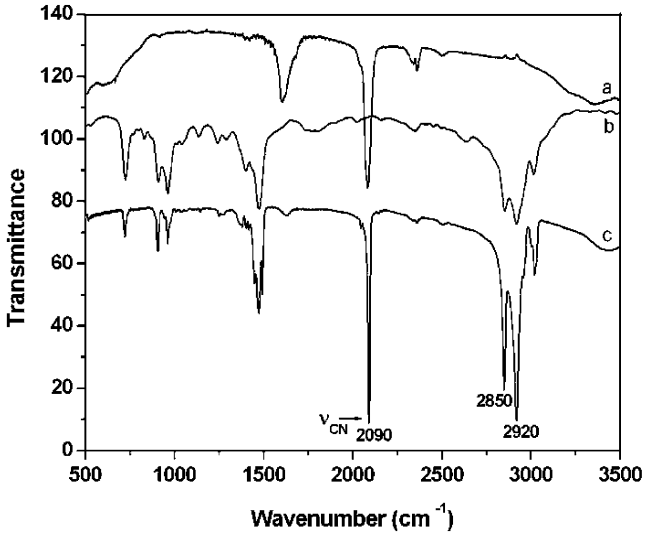

Figure 8. FTIR spectra of $K_4[Re_6Te_8(CN)_6]$ (a), CTABr (b) and C_{16}-$Re_6Te_8(CN)_6$ (c). C≡N and C–H modes are observed in **2**.

The energy dispersive X-ray spectroscopy (EDX) analysis shows the Re/Te ratio in the material to be very close to 3:4, agreeing with the expected ratio for the $[Re_6Te_8]^{2+}$ core. This, together with the presence of the cyanide group mentioned above, indicates that cluster $[Re_6Te_8(CN)_6]^{4-}$ is intact in the material.

The thermochemical properties of **2** were investigated using thermogravimetric analysis (TGA). Figure 9 indicates that no appreciable weight loss occurs up to 250 °C. Rather, the weight loss occurs predominantly from 250 to 450 °C. This weight loss of about 30% indicates decomposition of the surfactant $[C_{16}H_{33}N(CH_3)_3^+]$ from $[C_{16}H_{33}N(CH_3)_3]_4$-$[Re_6Te_8(CN)_6]$ (**2**). Single crystal X-ray analysis, IR, EDX

and TGA analysis confirm the chemical formula of $[C_nH_{2n+1}N(CH_3)_3]_4[Re_6Q_8(CN)_6]$ (Q = S, Se, Te). This type of formula was also observed in previously reported lamellar phases prepared from the clusters and the surfactants, and resulted from the cationic exchange reaction.[4–11]

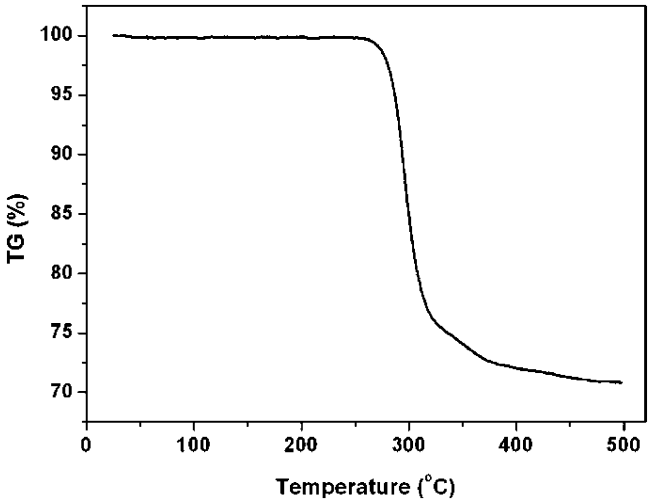

Figure 9. Thermogravimetric analysis of **2**. Weight loss of **2** is about 30%.

The fluorescence property of **2** was also investigated (Figure 10). Recently, others have studied the spectroscopic and photophysical properties of Re_6Q_8 clusters (Q = S, Se, Te).[17] The compound shows a behavior similar to that of the rhenium cluster itself; a solid sample of compound **2** shows an emission maximum at 742.4 nm with excitation at 463 nm. The emission maximum of **2**, at 754.8 nm, is found at 12 nm shorter wavelengths relative to that of $K_4[Re_6Te_8(CN)_6]$.

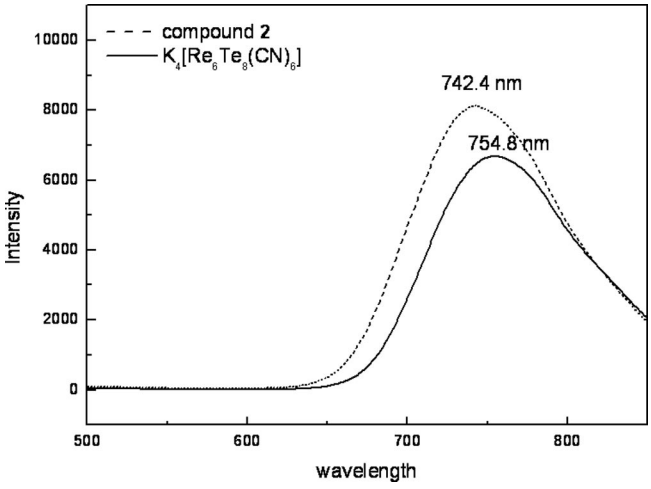

Figure 10. Solid-state emission (λ_{exc} = 463 nm) spectra of **2** and $K_4[Re_6Te_8(CN)_6]$ (from top to bottom). The maxima are observed at 742.4 and 754.8 nm, respectively.

The absorption properties of the solid phases were investigated by diffuse-reflectance solid-state UV/Vis spectroscopy. In general, chalcogenide materials have narrower energy bandgaps than oxides.[3b] The bandgaps of **2**, **4** and **5** are 2.03, 2.25 and 2.43 eV, respectively (shown in Figure 11), with these values decreasing with an increasing atomic number of chalcogen capped on the hexarhenium cluster. The bandgaps of the parent rhenium chalcogenide compounds are 1.86, 2.11 and 2.36 eV for $K_4[Re_6Te_8(CN)_6]$, $K_4[Re_6Se_8(CN)_6]$ and $K_4[Re_6S_8(CN)_6]$, respectively.

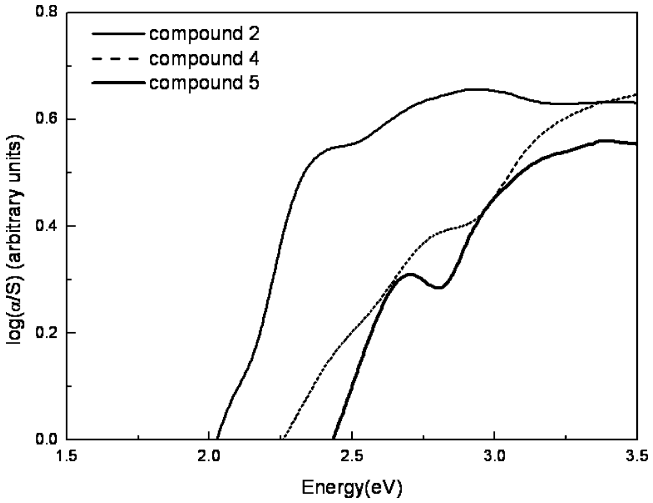

Figure 11. Solid-state UV/Vis spectra of **2**, **4**, and **5**. Absorption data were calculated from the reflectance data using the Kubelka–Munk function: $\alpha/S = (1 - R)^2/2R$, where R is the reflectance at a given wavenumber, α is the absorption coefficient, and S is the scattering coefficient. The bandgap energy is 2.03, 2.25, and 2.43eV for **2**, **4**, and **5**, respectively.

Conclusion

We synthesized new non-oxidic semiconducting and luminescent mesostructured materials by the surfactant-templated assembly of the octahedral rhenium cluster $[Re_6Q_8(CN)_6]^{4-}$ (Q = Te, Se and S) anions an H_2O/acetone medium at room temperature. This new family represents the first example of an octahedral cluster–surfactant hybrid, analogous to a tetrahedral $[Ge_4S_{10}]^{4-}$-containing mesostructured family, with a highly ordered lamellar structure. Further studies under different synthetic conditions such as hydrothermal and complex formations with various transition metals for new structural and physicochemical properties are currently underway.

Experimental Section

Starting Materials: The compound $K_4[Re_6Te_8(CN)_6]$ was synthesized by treating Re_2Te_5 with KCN. In addition, the compounds $K_4[Re_6Q_8(CN)_6]$ (Q = Se, S) were synthesized by treating of Re_2Te_5 with KCN, and Se or S, respectively, as described previously.[18] The powder X-ray diffraction patterns agree well with the powder patterns calculated from the single-crystal data of $K_4[Re_6Q_8(CN)_6]$ (Q = Te, Se, S). All other commercial reagents were used as received.

Synthesis of $[C_nH_{2n+1}N(CH_3)_3]_4[Re_6Q_8(CN)_6]$ (n = 14, 16, 18; Q = S, Se, Te; 1–5): $K_4[Re_6Q_8(CN)_6]$ (Q = S, Se, Te) (0.040 mmol) was dissolved in H_2O (1 mL). In a separate flask, the surfactant (0.36 g)

{TTABr [tertradecyltrimethylammonium bromide, $C_{14}H_{29}N(CH_3)_3$-Br], 1.1 mmol, for **1**; CTABr [cetyltrimethylammonium bromide, $C_{16}H_{33}N(CH_3)_3Br$], 1.0 mmol, for **2**, **4** and **5**; OTABr [octadecyltrimethylammonium bromide, $C_{18}H_{37}N(CH_3)_3Br$], 0.92 mmol for **3**} was dissolved in H_2O/acetone (3:2 mL). When the solutions of $K_4[Re_6Q_8(CN)_6]$ and the surfactant were combined, a red-brown solid formed immediately. The mixture was stirred at room temperature for 5 h. The solid was then isolated by filtration, washed with warm water and dried in an oven at 70 °C. $[C_{14}H_{29}N(CH_3)_3]_4[Re_6Te_8(CN)_6]$ (**1**), $[C_{16}H_{33}N(CH_3)_3]_4[Re_6Te_8(CN)_6]$ (**2**), $[C_{18}H_{37}N(CH_3)_3]_4[Re_6Te_8(CN)_6]$ (**3**), $[C_{16}H_{33}N(CH_3)_3]_4[Re_6Se_8(CN)_6]$ (**4**) and $[C_{16}H_{33}N(CH_3)_3]_4[Re_6S_8(CN)_6]$ (**5**) were obtained. Orange, platelake crystals of **1** and **4** were obtained by slow concentration of the solutions. X-ray data of **1** and **4** were collected for single-crystal structure determinations.

X-ray Crystallography: Single-crystal X-ray analysis was carried out with a Bruker SMART APEX CCD diffractometer using Mo-K_α radiation (λ = 0.71073 Å). The data were collected at room temperature by the standard technique. The CCD data were integrated and scaled using SAINT PLUS.[19] Absorption corrections were made empirically using SADABS. The structure was solved and refined using the SHELXTL program set.[20] The crystallographic data for compounds **1** and **4** are listed in Table 1. Selected bond lengths and angles are listed in Tables 2 and 3 for compounds **1** and **4**, respectively. CCDC-659848 (for **1**) and -659849 (for **4**) contain the supplementary crystallographic data for this paper. These data can be obtained free of charge from The Cambridge Crystallographic Data Centre via www.ccdc.cam.ac.uk/data_request/cif.

Table 2. Selected bond lengths [Å] and angles [°] for **1**.[a]

Re–Re	2.6819(16)–2.6926(17)
Re–Te	2.689(2)–2.709(2)
Re–C(cyano)	1.96(2)–2.09(3)
C–N(cyano)	1.21(3)–1.25(2)
N–C(surfactant)	1.47(2)–1.52(2)
C–C(surfactant)	1.41(4)–1.56(3)
C–H(surfactant head)	0.9600
C–H(surfactant tail)	0.9700
Re(1)#1-Re(3)–Re(2)	60.00(3)
Re(2)#1-Re(3)–Re(2)	90.06(4)
Re(3)–Te(6)–Re(2)#1	59.84(4)
N(1)–C(1)–Re(1)	178.0(18)
C(11)–N(11)–C(13)	109.5(16)
C(15)–C(16)–C(17)	115(2)
C(22)–N(12)–C(21)	110.3(17)
C(29)–C(28)–C(27)	120(3)
H(11A)–C(11)–H(11B)	109.5
H(21A)–C(21)–H(21B)	109.5
C(15)–C(14)–H(14B)	108.2
C(25)–C(24)–H(24B)	108.1

[a] Symmetry transformations used to generate equivalent atoms: #1: $-x$, $-y$, $-z$ + 1.

Thermogravimetric Analyses (TGA): TGA data were obtained under a constant N_2 flow with a heating rate of 10 °C/min in the SETRAM LABSYS TG system.

Transmission Electron Microscopy (TEM): High-resolution transmission electron micrographs were acquired with a JEOL JEM-3010 instrument (300 kV).

Spectroscopic Techniques: The emission spectra were recorded in the wavelength range of 500–850 nm with an F-4500 FL spectrophotometer. An Xe lamp was used as a light source to emit an intense and relatively stable radiation in a continuous range of 200–800 nm. The excitation slit width and the emission slit width were 5.0 nm, and the scan speed was 1200 nm/min. FT-IR spectra were obtained at room temperature with a BIORAD FTS 135 spectrometer in the range of wavenumbers from 4000 to 400 cm^{-1} at a resolution of 8 cm^{-1} with 16 scan times. The UV/Vis spectrum was recorded with a JASCO V-550 spectrophotometer. The response was medium, the scanning speed was 400 nm/min, and the bandwidth was 5.0 nm.

Table 3. Selected bond lengths [Å] and angles [°] for **4**.[a]

Re–Re	2.6331(12)–2.6428(11)
Re–Se	2.5151(18)–2.5392(18)
Re–C(cyano)	2.123(17)–2.145(19)
C–N(cyano)	1.130(18)–1.161(19)
N–C(surfactant)	1.46(2)–1.540(2)
C–C(surfactant)	1.44(3)–1.56(2)
C–H(surfactant head)	0.9600
C–H(surfactant tail)	0.9700
Re(2)–Re(3)–Re(1)#1	60.00(4)
Re(1)–Re(3)–Re(1)#1	90.05(5)
Re(2)–Se(7)–Re(1)	62.90(5)
N(1)–C(1)–Re(1)	175.7(14)
C(117)–N(11)–C(11)	109.4(12)
C(112)#2-C(111)–C(110)	118.4(17)
C(218)–N(21)–C(217)	109.4(13)
C(212)–C(213)–C(214)	118.4(15)
H(11C)–C(118)–H(11D)	109.5
H(21G)–C(219)–H(21H)	109.5
C(14)–C(14)–H(13A)	108.9
C(27)–C(28)–H(28A)	108.9

[a] Symmetry transformations used to generate equivalent atoms: #1: $-x$, $-y$, $-z$ + 1; #2: $-x$ + 2, $-y$, $-z$.

Acknowledgments

This research was supported by the SRC program of the Korea Science and Engineering Foundation (KOSEF), through the Center for Intelligent Nano-Bio Materials at Ewha Womans University (grant R11-2005-008-00000-0), and by the Ministry of Science and Technology (MOST) of Korea.

[1] a) C. T. Kresge, M. Leonowicz, W. J. Roth, J. C. Vartuli, J. C. Beck, *Nature* **1992**, *359*, 710–712; b) J. S. Beck, J. C. Vartuli, W. J. Roth, M. E. Leonowicz, C. T. Kresge, K. D. Schmitt, C. Chu, D. H. Olson, E. W. Sheppard, S. B. McCullen, J. B. Higgins, J. L. Schlenker, *J. Am. Chem. Soc.* **1992**, *114*, 10834–10843.

[2] a) Q. Huo, D. I. Margolese, G. D. Stucky, *Chem. Mater.* **1996**, *8*, 1147–1160; b) H. I. Lee, C. Pak, S. H. Yi, J. K. Shon, S. S. Kim, B. G. So, H. Chang, J. E. Yie, Y. U. Kwon, J. M. Kim, *J. Mater. Chem.* **2005**, *15*, 4711–4717.

[3] a) M. J. MacLachlan, N. Coombs, G. A. Ozin, *Nature* **1999**, *397*, 681–684; b) P. N. Trikalitis, K. K. Rangan, T. Bakas, M. G. Kanatzidis, *Nature* **2001**, *410*, 671–675; c) S. D. Korlann, A. E. Riley, B. L. Kirsch, B. S. Mun, S. H. Tolbert, *J. Am. Chem. Soc.* **2005**, *127*, 12516–12527.

[4] a) F. Bonhomme, M. G. Kanatzidis, *Chem. Mater.* **1998**, *10*, 1153–1159; b) M. Wachhold, M. G. Kanatzidis, *Chem. Mater.* **2000**, *12*, 2914–2923; c) K. K. Rangan, M. G. Kanatzidis, *Inorg. Chim. Acta* **2004**, *357*, 4036–4044.

[5] J. Li, B. Marler, H. Kessler, M. Soulard, S. Kallus, *Inorg. Chem.* **1997**, *36*, 4697–4701.

[6] G. G. Janauer, A. D. Dobley, P. Y. Zavalij, M. S. Whittingham, *Chem. Mater.* **1997**, *9*, 647–649.

[7] G. G. Janauer, A. Dobley, J. Guo, P. Zavalij, M. S. Whittingham, *Chem. Mater.* **1996**, *8*, 2096–2101.
[8] M. Nyman, D. Ingersoll, S. Singh, F. Bonhomme, T. M. Alam, C. J. Brinker, M. A. Rodriguez, *Chem. Mater.* **2005**, *17*, 2885–2895.
[9] A. Stein, M. Fendorf, T. P. Jarvie, K. T. Mueller, A. J. Benesi, T. E. Mallouk, *Chem. Mater.* **1995**, *7*, 304–313.
[10] A. Taguchi, T. Abe, M. Iwamoto, *Microporous Mesoporous Mater.* **1998**, *21*, 387–393.
[11] J. Do, A. J. Jacobson, *Chem. Mater.* **2001**, *13*, 2436–2440.
[12] a) J. C. P. Gabriel, K. Boubekeur, S. Uriel, P. Batail, *Chem. Rev.* **2001**, *101*, 2037–2066; b) H. D. Selby, Z. Zheng, *Comments Inorg. Chem.* **2005**, *26*, 75–102; c) Y. V. Mironov, N. G. Naumov, S. G. Kozlova, S. J. Kim, V. E. Fedorov, *Angew. Chem. Int. Ed.* **2005**, *44*, 6867–6871.
[13] a) Y. Kim, S. K. Choi, S.-M. Park, W. Nam, S.-J. Kim, *Inorg. Chem. Commun.* **2002**, *5*, 612–615; b) Y. Kim, S.-M. Park, W. Nam, S.-J. Kim, *Chem. Commun.* **2001**, 1470–1471; c) Y. Kim, S. Kim, S.-J. Kim, M. K. Lee, M. Kim, H. Lee, C. S. Chin, *Chem. Commun.* **2004**, 1692–1693.
[14] a) M. V. Bennett, L. G. Beauvais, M. P. Shores, J. R. Long, *J. Am. Chem. Soc.* **2001**, *123*, 8022–8032; b) L. G. Beauvais, M. P. Shores, J. R. Long, *J. Am. Chem. Soc.* **2000**, *122*, 2763–2772.
[15] L. Peng, J. Yu, Y. Li, R. Xu, *Chem. Mater.* **2005**, *17*, 2101–2107.
[16] R. A. Vaia, R. K. Teukolsky, E. P. Giannelis, *Chem. Mater.* **1994**, *6*, 1017–1022.
[17] T. G. Gray, C. M. Rudzinski, E. E. Meyer, R. H. Holm, D. G. Nocera, *J. Am. Chem. Soc.* **2003**, *125*, 4755–4770.
[18] Y. V. Mironov, J. A. Cody, T. E. Albrecht-Schmitt, J. A. Ibers, *J. Am. Chem. Soc.* **1997**, *119*, 493–498.
[19] Bruker, *SMART*, *SAINT*, Bruker AXS Inc., Madison, Wisconsin, USA, **1997**.
[20] Bruker, *SHELXTL*, Version 5.10, Bruker AXS Inc., Madison, Wisconsin, USA, **1998**.

Received: October 17, 2007
Published Online: December 20, 2007

